Photochemistry of the CpNiNO Complex. A Theoretical Study Using Density Functional Theory

P. Boulet,[†,‡,§] H. Chermette,*[,‡,§] and J. Weber[†]

Département de Chimie Physique, Université de Genève, 30 quai E-Ansermet, CH-1211 Genève 4, Suisse, Laboratoire de Chimie-Physique Théorique, Université Claude Bernard Lyon 1, Bat. 210, 43 Bd du 11 novembre 1918, 69622 Villeurbanne Cedex, France, and Institut de Recherches sur la Catalyse, CNRS UPR 5401, 69626 Villeurbanne Cedex, France

Received May 9, 2001

The photochemistry of the CpNiNO complex has been investigated using density functional theory. The whole potential energy curve along the NiNO angle coordinate is presented for the first time with both ground and metastable states, and transition states connecting the minima. The excited states of the GS, MS_I, and MS_{II} species have been calculated using time-dependent density functional theory. Furthermore, the structure of the excited states pertaining to the photochemistry of CpNiNO has been optimized. From these results it is shown that the backward GS ← MS_{II} ← MS_I reaction is more efficient than the forward GS → MS_{II} → MS_I scheme.

I. Introduction

Cyclopentadienyl-nitrosyl-nickel (CpNiNO) belongs to the transition metal nitrosyl compounds, a class of molecular complexes possessing metastable states which are potential candidates for optical information storage. Their interest lies in their long-lived metastable states which are easily obtained by light irradiation.

The first experimental elucidation of the UV−vis spectrum of CpNiNO was undertaken by Crichton and Rest in 1977.[1] These authors showed that irradiation with UV light produces a decrease of the IR band of the nitrosyl ligand (1839 cm^{-1}) and the appearance of a new band located at 1392 cm^{-1}. No free NO radical could be detected during the experiment. Furthermore, irradiation of the sample with a lower energetic beam implies the regeneration of the NO stretching mode. From UV−vis, EXAFS, and FTIR experiments, Chen et al.[2] have evidenced the photoexcitation of the ground state CpNiNO into a bent metastable state. However, they could neither characterize the electronic excitations which are responsible for the forward and backward reactions nor elucidate the structure of the metastable state. This problem has been tackled by Coppens et al. from an experimental study of Cp*NiNO combining low-temperature X-ray crystallography and photochemistry,[3,4] where Cp* stands for the pentamethylcyclopentadienyl ring. In addition, they investigated the ground state and the first and second metastable states of CpNiNO by density functional theory. Finally, it is only very recently that the linear MS_I metastable state of CpNiNO, namely, CpNiON, has been experimentally detected[5] from IR spectroscopy.

We present in this paper a detailed theoretical study of the ground state (GS), metastable states (MS_I and MS_{II}), and excited states of the CpNiNO complex. The rest of the paper is organized as follows: After having presented some theoretical details, we describe the complete potential energy curve as a function of the NiNO rotation angle. In the next part, the calculated absorption spectra of the GS, MS_I, and MS_{II} species are compared to the experimental ones. The following section is devoted to the explanation of the forward and backward reactions on the basis of our results. Finally, we end up with some concluding remarks.

II. Theoretical Approach

The density functional theory[6] within the Kohn−Sham methodology[7] has been used. Becke's exchange functional[8] and Perdew's correlation functional[9] (B88P86) have been employed in the generalized gradient approximation (GGA). The calculations have been performed using the ADF99[10,11] program package. The basis set is of triple-ζ quality with polarization functions on the N, O, and H atoms (basis IV according to ADF terminology). For the integration grid (number of points for the numerical integration), the parameter has been fixed to 5.0.

For the calculation of the excited states of CpNiNO, both the ΔSCF method[12,13] and the time-dependent density functional theory (TD-DFT)[14,15,16] within the adiabatic approximation have been used. For

* To whom correspondence should be addressed. E-mail: cherm@catalyse.univ-lyon1.fr.

† Université de Genève.

‡ Université Claude Bernard Lyon 1.

§ Institut de Recherches sur la Catalyse.

(1) Crichton, O.; Rest, A. J. *J. Chem. Soc., Dalton Trans.* **1977**, *10*, 986.
(2) Chen, L. X.; Bowman, M. K.; Wang, Z.; Montano, P. A.; Norris, J. R. *J. Phys. Chem.* **1994**, *98*, 9457.
(3) Coppens, P.; Fomitchev, D. V.; Carducci, M. D.; Culp, K. *J. Chem. Soc., Dalton Trans.* **1998**, 865.
(4) Fomitchev, D. V.; Furlani, T. R.; Fomitchev, D. V. *Inorg. Chem.* **1998**, *37*, 1519.
(5) Schaiquevich, P. S.; Güida, J. A.; Aymonino, P. J. *Inorg. Chim. Acta* **2000**, *303*, 277.
(6) Hohenberg, P.; Kohn, W. *Phys. Rev. A* **1964**, *136*, 864.
(7) Kohn, W.; Sham, L. J. *Phys. Rev. A* **1965**, *140*, 1133.
(8) Becke, A. D. *Phys. Rev. A* **1988**, *38*, 3098.
(9) Perdew, J. P. *Phys. Rev. B* **1986**, *33*, 8822.
(10) Baerends, E. J.; Bérces, A.; Bo, C.; Boerrigter, P. M.; Cavallo, L.; Deng, L.; Dickson, R. M.; Ellis, D. E.; Fan, L.; Fischer, T. H.; Fonseca Guerra, C.; van Gisbergen, S. J. A.; Groeneveld, J. A.; Gritsenko, O. V.; Harris, F. E.; van den Hoek, P.; Jacobsen, H.; van Kessel, G.; Kootstra, F.; van Lenthe, E.; Osinga, V. P.; Philipsen, P. H. T.; Post, D.; Pye, C. C.; Ravenek, W.; Ros, P.; Schipper, P. R. T.; Schreckenbach, G.; Snijders, J. G.; Sola, M.; Swerhone, D.; te Velde, B.; Vernooijs, P.; Versluis, L.; Visser, O.; van Wezenbeek, E.; Wiesenekker, G.; Wolff, S. K.; Woo, T. K.; Ziegler, T. *ADF1999*. te Velde, G.; Bickelhaupt, F. M.; Baerends, E. J.; Fonseca Guerra, C.; van Gisbergen, S. J. A.; Snijders, J. G.; Ziegler, T. *J. Comput. Chem.* **2001**, *22*, 931.
(11) Fonseca Guerra, C.; Snijders, J. G.; te Velde, B.; Baerends, E. J. *Theor. Chem. Acc.* **1998**, *99*, 391.
(12) Ziegler, T.; Rauk, A.; Baerends, E. J. *Theor. Chim. Acta* **1977**, *43*, 261.
(13) Daul, C. *Int. J. Quantum Chem.* **1994**, *52*, 867.
(14) Gross, E. K. U.; Dobson, J. F.; Petersilka, M. In *Density Functional Theory of Time-Dependent Phenomena*, Topics in Current Chemistry; Nalewajski, R. F., Ed.; Springer: New York, 1996; Vol. 181.

10.1021/ic010489c CCC: $20.00
Published on Web 12/04/2001

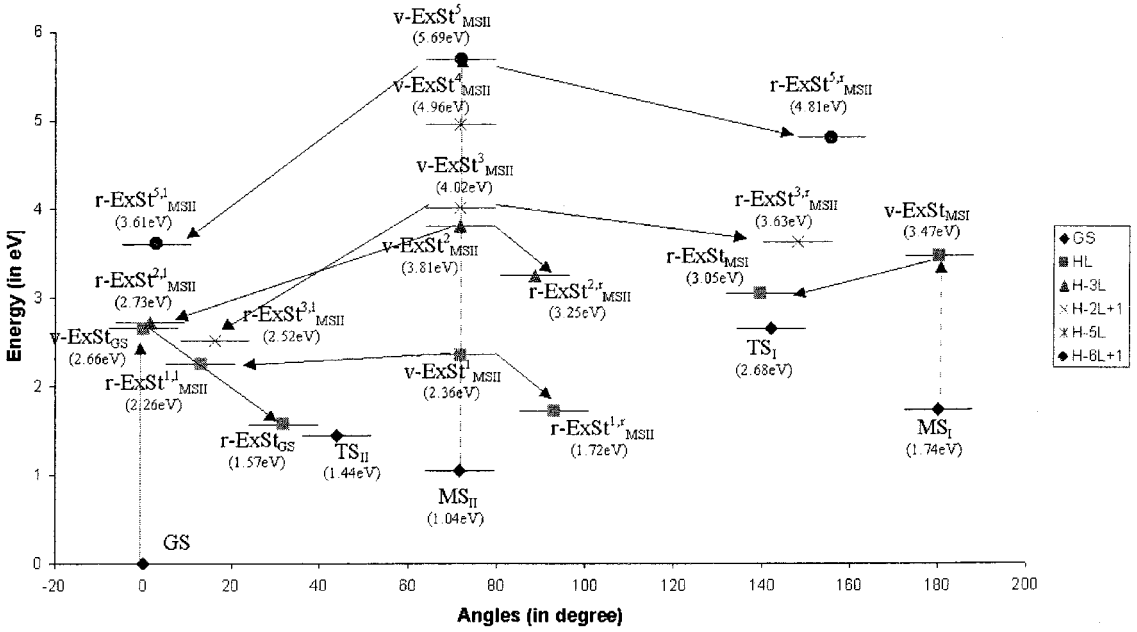

Figure 1. Ground and excited state potential energy curve of CpNiNO.

Chart 1. Ground (Global Minimum) and Metastable States (Local Minima) on the Potential Energy Curve of CpNiNO

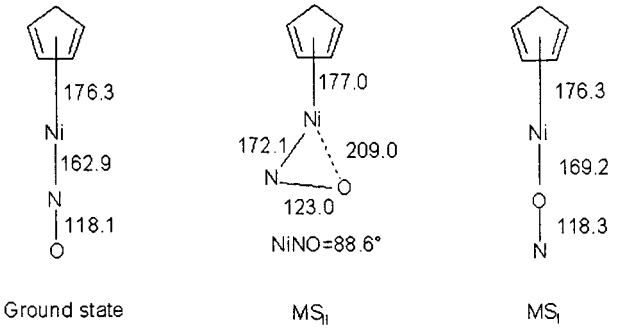

the remaining excited states, namely, those of the metastable states MS_{II} and MS_I, only the TD-DFT methodology has been used. In order to avoid the dramatic collapse of excitation energies calculated with an LDA potential,[17] the asymptotically well-behaved potential functional developed by van Leeuwen and Baerends (LB94)[18] has been used during the SCF procedure. The calculation of the coupling matrix has been performed using the adiabatic local density approximation (ALDA).

III. Results

A. Investigation of the Ground State Potential Energy Curve (PEC). 1. Qualitative Description of the PEC. The potential energy curve of the ground state CpNiNO complex is depicted in Figure 1. The reaction coordinate is the NiXN angle where X stands for a dummy atom located at the center of the NO bond. The ground state and metastable states are presented in Chart 1 together with their geometrical parameters (in picometers and degrees). It can be seen that the global minimum has a linear NiNO group of atoms (i.e., NiNO = 180°).

Table 1. IR Parameters of the GS, MS_{II}, and MS_I Species (cm^{-1})[a]

	GS	MS_{II}	MS_I
ν(NiN)	622 (636−644)[b]	731 (710)[b]	
ν(NO)	1815 (1786)[c]	1434 (1387)[d]	1713 (1576)[b]
δ(NiNO)	472 (489−492)[b]	405 (419)[b]	433
ν(NiO)			557

[a] The experimental wavenumbers are in parentheses. [b] Reference 5. [c] Reference 4. [d] Reference 2.

Therefore, its symmetry is C_{5v}. The structure of the ground state species has been elucidated by EXAFS spectroscopy[2] and by photocrystallographic experiment.[3,4] Calculated geometrical parameters will be compared to the most recent experimental data. The calculated parameters are in relatively good agreement with experimental ones. For instance, the experimental NiN bond distance is 161.4−162.0 pm, and the NiO one amounts to 279.5−279.7 pm (as the crystal unit cell contains two independent molecules, two values of each geometrical parameter have been measured). Our results are 162.9 and 281.0 pm, respectively. The NO bond length is of particular importance for the photochemistry of CpNiNO. The experimental estimation for the NO bond length is 117.7−118.1 pm. As can be seen in Chart 1, the calculated NO bond length amounts to 118.1 pm. Furthermore, the experimental IR spectrum of CpNiNO has also been characterized.[4] The frequency of the NO stretching mode amounts to 1786 cm^{-1} (see Table 1). The calculation of the IR spectrum has been performed, and the NO band is located at 1815 cm^{-1}. A good agreement between experiment and calculations is usually expected in DFT calculations (1% in our case),[19] which suggests that the effect of the surrounding environment may be neglected in our study.

The second minimum in Figure 1 corresponds to the first metastable state, conventionally named MS_{II}. The structure presents a bent NiNO group of atoms. Therefore, the symmetry of this species is no longer C_{5v} but C_s. The NiNO angle is calculated to amount to 88.6°. This angle is slightly lower than what was expected from X-ray experiment[4] (93.1°) but in full agreement with previous DFT calculations (88°).[3,4] The experimental IR spectrum of the MS_{II} complex[2] shows a drastic

(15) Casida, M. E. In *Time-Dependent Density-Functional Response Theory for Molecules*; Recent Advances in Density Functional Methods; Chong, D. P., Ed.; World Scientific: Singapore, 1995.
(16) Casida, M. E. In *Time-Dependent Density Functional Response Theory of Molecular Systems: Theory, Computational Methods and Functionals*; Recent Developments and Applications of Modern Density Functional Theory; Seminario, J. M., Ed.; Elsevier: Amsterdam, 1996.
(17) Jamorski, C.; Casida, M. E.; Salahub, D. R. *J. Chem. Phys.* **1996**, *104*, 5134.
(18) van Leeuwen, R.; Baerends, E. J. *Phys. Rev. A* **1994**, *49*, 2421.
(19) Chermette, H. *Coord. Chem. Rev.* **1998**, *178*−*180*, 699.

Chart 2. Transition States on the Potential Energy Curve of CpNiNO

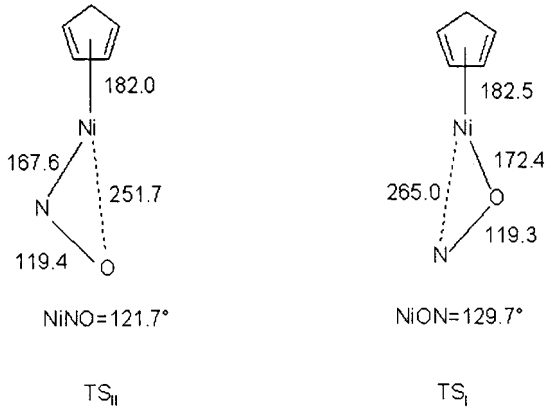

downshift of the NO stretching frequency (see Table 1) of 437 cm^{-1}. This shift is predicted to be smaller by our calculations (381 cm^{-1}). Upon rotation of the NO group we can notice (see Chart 1) that the NO bond length slightly elongates (by 4.9 pm), which results in the weakening of the bond strength. This explains the red shift of the NO vibration mode. The Ni−Cp distance remains unchanged during the rotation. Finally this structure is 1.05 eV higher in energy than the ground state complex.

The last local minimum in Figure 1 is the CpNiON complex denoted MS_I, and it corresponds to the metastable state with inverted NO atoms. As the NiON group of atoms is linear, the symmetry of CpNiON is C_{5v}. In Chart 1 one can see that from MS_{II} to MS_I the NO bond almost recovers the length of the ground state complex. Therefore, compared with the ground state, the calculated NO stretching frequency is slightly red-shifted by 102 cm^{-1} (Table 1). This is significantly smaller than the experimental red shift, which is equal to 248 cm^{-1}.[5] At present, we have no explanation for this discrepancy. This could be related to a weakness of the exchange-correlation functional for the description of the π bonds, as similar effects have been obtained with phosphorus-containing compounds[20] or cyano/isocyano-containing complexes.[21] The red shift is related to a weakening of the metal−NO bond when the N atom is permutated with the O atom. This should be correlated to an increase of this metal−ligand bond. In fact, upon rotation of the NO group, this trend is hidden because of the substitution of the N atom by the O one: since the covalent radii of the oxygen atom is greater than that of the nitrogen atom (at least in some databases), the metal−ligand bond distance decreases. The MS_I structure is 1.74 eV less stable than its isomer CpNiNO.

The ground and MS_{II} states are connected on the PEC by a transition state TS_{II} (see Chart 2). The energetic barrier between the GS and the MS_{II} species amounts to 1.44 eV. It is therefore expected that such a barrier cannot be overcome by thermal excitation (remember that the temperature of the experiment is 25 K in ref 4). As can be seen in Chart 2, the NiNO angle has, as expected, an intermediate value of 121.7°. Interestingly, the NO bond length is elongated in the TS_{II}, approaching its maximum elongation present in MS_{II}. More interestingly, the Ni−Cp distance is stretched in the transition state upon rotation of the NO group.

The second transition state TS_I (Chart 1) is located between the MS_{II} and the MS_I structures. The energetic barrier for the $MS_{II} \rightarrow MS_I$ transition is a little higher than that of the GS $\rightarrow$ MS_{II} one and amounts to 1.64 eV. It is worthwhile to note that the NO bond length, the Ni−Cp distance, and the NiON angle of TS_I are very similar to the corresponding ones in TS_{II}. Therefore, the difference in stability between both species is closely related to the difference in the Ni−O and Ni−N electronic interactions.

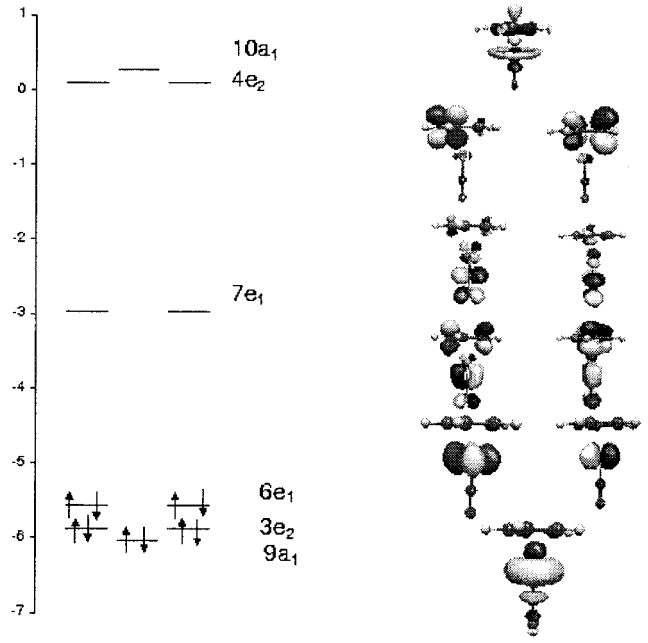

Figure 2. Ground state molecular orbitals of CpNiNO (C_{5v} symmetry). The isosurfaces are plotted at 0.05 au.

As a concluding remark, one can notice that the PEC of the CpNiNO complex is very similar to that of sodium nitroprusside.[22,23]

2. Description of the PEC in Terms of Molecular Orbital Interactions. The electronic configuration of the ground state CpNiNO around the Fermi level is $9a_1^2 3e_2^4 6e_1^4 7e_1^0 4e_2^0 10a_1^0$. The symmetry of the state is therefore $|^1A_1\rangle$. As shown in Figure 2 the HOMO (highest occupied molecular orbital) is mainly of ligand-type character. It is Cp−Ni and N−O π antibonding and Ni−N π bonding. The participation of the $d_{xz,yz}$ orbitals of Ni is remarkably marginal. As expected, the LUMO (lowest unoccupied molecular orbital) mainly accommodates the π^* NO orbital and is Cp−Ni, Ni−N, and N−O antibonding. The HOMO−LUMO energy gap is quite large and amounts to 2.61 eV. The HOMO−1 and HOMO−2 orbitals are of metal character ($d_{x^2-y^2,xy}$ and d_{z^2}) whereas the LUMO+1 corresponds to the Cp ligand π^* orbital and the LUMO+2 to the σ^* orbital. The $9a_1$ MO is slightly lower in energy than the $3e_2$ one. Finally, one may notice in Figure 2 the large gap between the LUMO and LUMO+1 orbitals (3.05 eV).

In Figure 3 are depicted the MOs near the Fermi level of the TS_{II}, MS_{II}, and TS_I species, respectively.

As the symmetry falls to C_s upon rotation of the NO group of atoms, the electronic configuration of TS_{II} is $|9a''^2 18a'^2 19a'^0 10a''^0; {}^1A'\rangle$. The $6e_1$ MO of the GS splits into the 9a″ and 18a′ MOs, and the $7e_1$ MO splits into the 19a′ and 10a″ MOs. The energy behavior of the orbitals from GS to TS_{II} can be explained in terms of overlap. Compared with the $6e_1$ MO of the GS, the

(20) Joantéguy, S.; Pfister-Guillouzo, G.; Chermette, H. *J. Phys. Chem. A* **1999**, *103*, 3505.
(21) Chermette, H. Unpublished results.
(22) Delley, B.; Schefer, J.; Woike, T. *J. Chem. Phys.* **1997**, *107*, 10067.
(23) Boulet, P.; Buchs, M.; Chermette, H.; Daul, C.; Gilardoni, F.; Rogemond, F.; Schläpfer, C. W.; Weber, J. *J. Phys. Chem. A* **2001**, *105*, 8991.

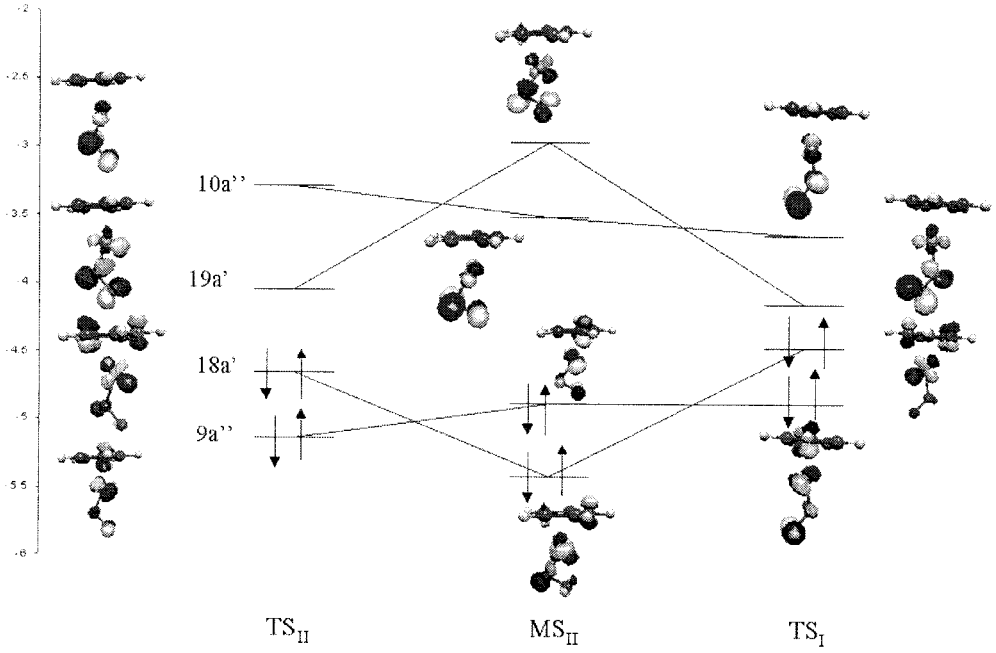

Figure 3. Molecular orbital evolution between TS_{II}, MS_{II}, and TS_I of CpNiNO (C_s symmetry). The isosurfaces are plotted at 0.05 au.

Table 2. Relative Energies and HOMO−LUMO Gaps of the GS, MS_{II}, MS_I, TS_{II}, and TS_I Species[a]

	GS	TS_{II}	MS_{II}	TS_I	MS_I
energies	0.00	1.81	1.42	2.80	1.61
gap	2.61	0.61	1.36	0.31	1.75

[a] All values are in electronvolts.

destabilization of the 9a″ MO of TS_{II} is due to the slight antibonding overlap between the nitrogen atom and the metal center (this interaction is completely bonding in the GS; see Figure 2). The destabilization of the 18a′ MO of TS_{II} is even more pronounced and results from the same kind of interaction. On the contrary, the MOs emerging from the splitting of the LUMO of the GS are stabilized. The 19a′ MO is the most stabilized one as a bonding character appears between the metal center and the nitrogen atom. The stabilization of the 10a″ MO is due to the electron density relocalization from the Cp ligand to the Ni atom and the nitrosyl ligand. Therefore, the antibonding character between the Cp ligand and the metal center vanishes. These electronic rearrangments lead to a tremendous decrease of the HOMO−LUMO gap in the TS_{II} species (0.61 eV, see Table 2). This last trend, initiated in TS_{II}, is also observed for the MS_{II}, TS_I, and MS_I species.

From TS_{II} to MS_{II} the HOMO and HOMO−1 orbitals cross each other. This crossing is also observed between the LUMO and LUMO+1 orbitals. As depicted in Figure 3, it is obvious that the stabilization of both the 18a′ and the 10a″ orbitals is due to the bonding interaction between the Ni center and the oxygen atom. Consequently, the HOMO orbital of MS_{II} is a η^2 di-σ type orbital. On the contrary, the destabilization of both the 9a″ and the 19a′ orbitals is induced by the antibonding character of the Ni−O interaction. The HOMO−LUMO gap of the species amounts to 1.36 eV (Table 2).

Along the $MS_{II} \rightarrow TS_I$ path we may observe (Figure 3) that, as for the $TS_{II} \rightarrow MS_{II}$ transition, the same orbitals cross each other. Therefore, the electronic configuration of TS_I is similar to that of TS_{II}. Again, these crossings can be rationalized by the favorable or unfavorable overlaps between the nitrosyl ligand and the metal center. Consequently, one can underline that the electron density structures of TS_I and TS_{II} are qualitatively similar (compare the topology of the MOs in Figure 3). Furthermore the HOMO−LUMO gap of TS_I has roughly the same magnitude (0.31 eV, Table 2) as that of TS_{II} (0.61 eV). The relative stability of both the TS_I and TS_{II} species cannot be explained on the basis of the topology of the respective molecular orbitals. A comparison of the electronic interactions can give more insight in the rationalization of this problem. As seen in Table 3, both the electrostatic interactions and the Pauli repulsion are larger in TS_{II} than in TS_I, corresponding to a larger steric repulsion. However, because of larger orbital interactions, the TS_{II} species is definitely more stable than TS_I. This is mainly because the metal−N bond distance of TS_{II} is shorter than the metal−O bond distance of TS_I (all other bonds remaining equal elsewhere). Consequently, the molecular orbital interactions are more stabilizing in TS_{II} than in TS_I.

Table 3. Analysis of the Relative Stability of the GS, MS_{II}, MS_I, TS_{II}, and TS_I Species through Fragment Decomposition Analysis[a]

	steric repulsion			
	Pauli repulsion	electrostatic interaction	orbital interaction	bonding energy
GS	11.472	−2.678	−11.732	−2.94
TS_{II}	11.205	−2.599	−11.491	−2.88
MS_{II}	11.089	−2.610	−11.377	−2.90
TS_I	11.090	−2.549	−11.378	−2.84
MS_I	11.282	−2.610	−11.544	−2.87

[a] All values are in atomic units.

Finally the last structure on the PEC is the isomer of the ground state CpNiNO species, namely, the CpNiON complex. The MOs of this metastable state are depicted in Figure 4. Similarly to the ground state CpNiNO, the NiNO group of atoms is linear and, consequently, the symmetry of this species is C_{5v}. The electronic structure of CpNiON is $|9a_1^2 3e_2^4 6e_1^4 7e_1^0 10a_1^0 4e_2^0; {}^1A_1\rangle$. The major difference between both isomers is the permutation of the $4e_2$ and the $10a_1$ MOs. Similarly to the TS_I and TS_{II} species, the greater stabilization of the ground state compared with that of the MS_I structure results from the balanced equilibrium between steric and orbital interactions (Table 3).

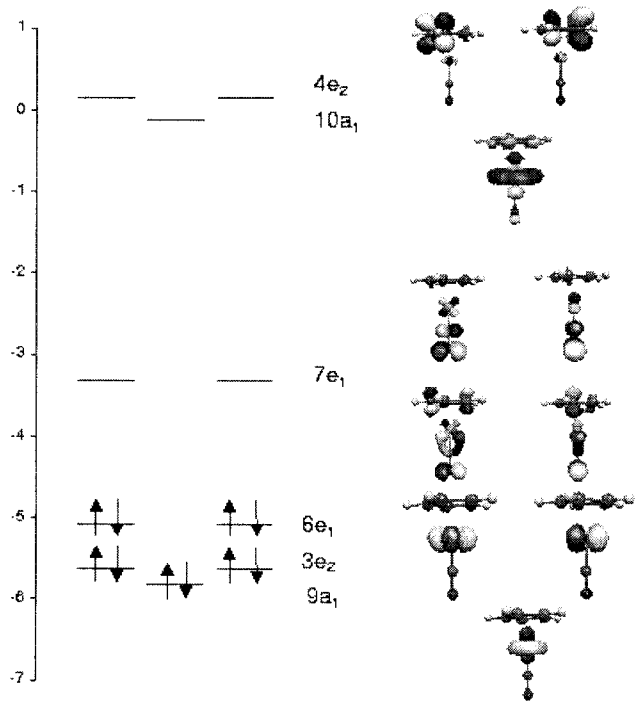

Figure 4. Molecular orbitals of CpNiON (C_{5v} symmetry). The isosurfaces are plotted at 0.05 au.

It is worth noting that the changes in the HOMO−LUMO gap when going from GS to MS_I follow roughly the maximum hardness principle, which states that the higher the hardness (i.e., the gap), the more stable the compound.[25−28] One can see easily in Table 2 that the largest gaps belong to the (meta)-stable structures, and the lowest gaps are found in the transition state structures. Finally the GS exhibits the largest gap among the three stable structures. However the MS_{II} state exhibits a lower gap than MS_I, although being a little more stable. This trend is responsible for the red shift in the electronic transitions of MS_I in comparison with the corresponding ones in the GS (see Tables 4−6).

B. Excited States. 1. Excited States of the Ground State CpNiNO. The experimental absorption spectrum of CpNiNO[2] features four bands. The former two, which are located at 2.68 and 3.22 eV, have very similar intensities and are about 100 times less intense than the latter two bands, which are found at 4.43 and 6.20 eV.

According to TD-DFT calculations (Table 4), the first two peaks are a combination of mainly two transitions, namely, the $9a_1 \rightarrow 7e_1$ one and the $3e_1 \rightarrow 7e_1$ one, with a reversed contribution in each peak. These excited states are both of E_1 symmetry. It is also worthwhile noting that the shift in energy between these peaks is well reproduced by TD-DFT. The description of the excitation energies by the ΔSCF procedure is satisfactory. The greater deviation from experiments amounts to 0.45 eV. On the contrary, the calculated intensities of these transitions, not given in Table 4, are not reliable, probably because of the important mixture of determinants in the transitions.

Table 4. Optical Absorption of the Ground State CpNiNO Complex

			LB94//B88P86			exptl[d]	
sym	MO[a]	ΔSCF	energy (eV)	f (au)[b]	%[c]	energy (eV)	int[e]
E_1	$9a_1 \rightarrow 7e_1$	3.25	3.08	4.0×10^{-4}	87	2.68 (2.85[f])	w
	$3e_2 \rightarrow 7e_1$				7		
E_1	$9a_1 \rightarrow 7e_1$	3.95	3.52	4.0×10^{-4}	13	3.22 (3.40[f])	w
	$3e_2 \rightarrow 7e_1$				86		
A_1	$6e_1 \rightarrow 7e_1$	3.69	4.24	0.4	70	4.43 (4.27−4.77[f])	s
	$5e_1 \rightarrow 7e_1$				24		
E_1	$6e_1 \rightarrow 10a_1$	5.98	6.42	1.2×10^{-4}	94		
E_1	$3e_2 \rightarrow 4e_2$		6.41	1.7×10^{-2}	78		
	$8a_1 \rightarrow 7e_1$				10		
E_1	$8a_1 \rightarrow 7e_1$	6.39	5.97	3.6×10^{-2}	54	6.20	s
	$6e_1 \rightarrow 4e_2$				44		
A_1	$4e_1 \rightarrow 7e_1$		6.00	0.25	72		
	$5e_1 \rightarrow 7e_1$				18		
A_1	$9a_1 \rightarrow 10a_1$	7.16	7.22	9.0×10^{-4}	86		
E_1	$2e_2 \rightarrow 7e_1$		5.54	$\ll 10^{-4}$	100		
A_1	$3e_2 \rightarrow 4e_2$		6.74	0.5	70		
	$6e_1 \rightarrow 7e_1$				12		
	$5e_1 \rightarrow 7e_1$				10		
A_1	$6e_1 \rightarrow 8e_1$		7.27	3.5×10^{-2}	86		
	$9a_1 \rightarrow 10a_1$				12		

[a] Molecular orbital. [b] Oscillator strength. [c] Percentage of the corresponding electron configuration in the total density. [d] Reference 2. [e] w = weak and s = strong. [f] Hg lines used in ref 2 to study the wavelength dependence of the GS → MS_{II} reaction.

Table 5. Optical Absorption of the MS_{II} Complex

		LB94//B88P86			exptl[d]
sym	MO[a]	energy (eV)	f (au)[b]	%[c]	energy (eV)
A′	$9a'' \rightarrow 10a''$	1.66	7.2×10^{-3}	83	1.46
	$18a' \rightarrow 19a'$			14	
A′	$8a'' \rightarrow 10a''$	2.77	0.6×10^{-3}	70	2.27[e]
	$18a' \rightarrow 19a'$			27	
A′	$17a' \rightarrow 19a'$	3.32	0.4×10^{-2}	37	
	$18a' \rightarrow 19a'$			26	
	$16a' \rightarrow 19a'$			21	
	$8a'' \rightarrow 10a''$			9	
A′	$7a'' \rightarrow 10a''$	4.00	7.6×10^{-2}	71	3.71[e]
	$18a' \rightarrow 19a'$			9	
	$16a' \rightarrow 19a'$			7	
	$17a' \rightarrow 19a'$			2	
A′	$15a' \rightarrow 19a'$	4.15	0.15	26	3.96/4.10[e]
	$17a' \rightarrow 19a'$			18	
	$18a' \rightarrow 19a'$			13	
	$16a' \rightarrow 19a'$			12	
	$8a'' \rightarrow 10a''$			11	
	$7a'' \rightarrow 10a''$			11	
A″	$9a'' \rightarrow 20a'$	5.34	0.0117	81	
	$12a' \rightarrow 10a''$			8	
A′	$9a'' \rightarrow 11a''$	5.46	0.0228	78	
	$18a' \rightarrow 20a'$			15	
A′	$14a' \rightarrow 19a'$	5.61	0.0172	60	
	$5a'' \rightarrow 10a''$			32	
A′	$5a'' \rightarrow 10a''$	5.92	0.0158	55	
	$14a' \rightarrow 19a'$			37	

[a] Molecular orbitals. [b] Oscillator strength. [c] Percentage of the corresponding electron configuration in the total density. [d] Reference 2. [e] Mercury lines used to excite the sample.

The experimental band located at 4.43 eV (calcd 4.24 eV) mainly corresponds to the HOMO−LUMO transition ($6e_1 \rightarrow 7e_1$) (see Table 4) with a minor contribution of the HOMO−3 → LUMO transition. It belongs to the A_1 symmetry. A high intensity for this excitation was expected as it is of ligand-to-ligand charge transfer type (σ-Cp to π^*-NO).

The last band (6.20 eV with E_1 symmetry) is composed of two transitions, namely, the HOMO−2 → LUMO and the

(24) Boulet, P.; Chermette, H.; Daul, C.; Gilardoni, F.; Rogemond, F.; Weber, J.; Zuber, G. *J. Phys. Chem. A* **2001**, *105*, 885.
(25) Chermette, H. *J. Comput. Chem.* **1999**, *20*, 129.
(26) Chattaraj, P. K. *Proc. Indian Natl. Sci. Acad. Part A* **1996**, *62*, 513.
(27) Pearson, R. G. *Chemical Hardness: Applications from Molecules to Solids*; Wiley-VCH: 1997.
(28) Chattaraj, P. K.; Poddar, A. J. *J. Phys. Chem. A* **1998**, *102*, 9944.

Table 6. Optical Absorption of the MS_I Complex

		LB94//B88P86		
sym	MO[a]	energy (eV)	*f* (au)[b]	%[c]
E_1	$9a_1 \rightarrow 7e_1$	2.47	3.0×10^{-4}	0.87
	$3e_2 \rightarrow 7e_1$			0.14
E_1	$3e_2 \rightarrow 7e_1$	2.83	1.0×10^{-4}	0.86
	$9a_1 \rightarrow 7e_1$			0.13
A_1	$6e_1 \rightarrow 7e_1$	3.73	0.4	0.62
	$5e_1 \rightarrow 7e_1$			0.32
A_1	$4e_1 \rightarrow 7e_1$	5.46	0.45	0.44
	$5e_1 \rightarrow 7e_1$			0.28
	$6e_1 \rightarrow 7e_1$			0.24
E_1	$6e_1 \rightarrow 4e_2$	5.59	2.4×10^{-2}	0.58
	$8a_1 \rightarrow 7e_1$			0.38
E_1	$6e_1 \rightarrow 10a_1$	5.84	3.1×10^{-3}	0.97
E_1	$3e_2 \rightarrow 4e_2$	6.09	2.2×10^{-2}	0.42
	$8a_1 \rightarrow 7e_1$			0.37
	$6e_1 \rightarrow 4e_2$			0.14
A_1	$4e_1 \rightarrow 7e_1$	6.11	0.2	0.42
	$3e_2 \rightarrow 4e_2$			0.36
	$5e_1 \rightarrow 7e_1$			0.10

[a] Molecular orbitals. [b] Oscillator strength. [c] Percentage of the corresponding electron configuration in the total density.

HOMO−1 → LUMO ones, with important contributions (55% and 44%, respectively). This band, which is located at 5.97 eV, is calculated to be roughly 10 times less intense than the band at 4.24 eV and overlaps with an even more intense band located at 6.0 eV which is estimated to be 7 times more intense. This band is also composed of two transitions, namely, the HOMO−6 ($4e_1$) → LUMO ($7e_1$) and the HOMO−3 ($5e_1$) → LUMO with respective contributions of 72% and 18%. Further on the spectrum (not measured experimentally) lies another intense band at 6.74 eV. This band has 22% of $\{5e_1,6e_1\}$ → LUMO ($7e_1$) excitation and 70% of HOMO−1 ($3e_2$) → LUMO+1 ($4e_2$).

From a theoretical point of view two points are important to notice. First, the whole spectrum predicted by TD-DFT looks a little bit shrunk. The energy of low-lying bands is overestimated while that of the higher ones is downshifted. This is quite an unusual trend for this method. Second, the ΔSCF results are not as reliable as the TD-DFT ones. Actually, the A_1 band, experimentally measured at 4.43 eV, is drastically downshifted involving an inversion in the order of the excited states. Usually, a much better agreement between TD-DFT and ΔSCF results is observed,[24] a trend which is not obtained in the case of the ground state of CpNiNO. Finally, when TD-DFT calculations are performed, one should take care that transitions involving rather low-lying occupied orbitals toward the first unoccupied orbital may contribute significantly to intense transitions.

2. Excited State of the First Metastable State MS_{II}. From experimental results,[2] only one band has been attributed to the absorption of the first metastable state MS_{II}. This is a broad band located at 1.46 eV with low intensity. The calculated UV spectrum (Table 5) assigns this band to the HOMO−LUMO ($9a'' \rightarrow 10a''$) transition with minor contribution from the HOMO−1 → LUMO+1 transition. In agreement with experiment, the intensity of this band is calculated to be small. In the region of the Hg lines used to excite the sample (2.27 eV) an absorption band of the MS_{II} species has been found (2.77 eV). The intensity of this transition lies in the same range of magnitude as the first one. The reason why these two bands have the same intensity is probably related to the fact that the HOMO and HOMO−3 orbitals mainly accommodate the nickel d electrons. Consequently, the low-energy part of the MS_{II} spectrum is similar to that of the ground state CpNiNO.

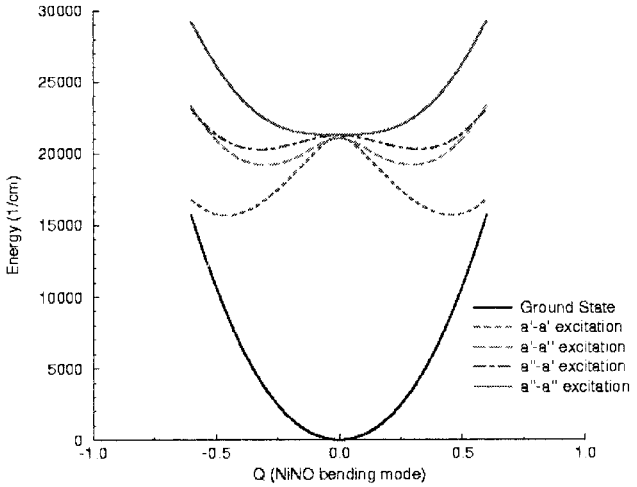

Figure 5. Evolution of the total energy of the HOMO−LUMO excited state of the ground state CpNiNO along the NiNO bending mode coordinate.

At higher energy, calculations show (see Table 5) that the MS_{II} species absorbs at 3.32, 4.00, and 4.15 eV, again in the region of the Hg lines. These bands mainly correspond to the promotion of inner electrons (HOMO−2, HOMO−5, and HOMO−6 orbitals, respectively) to the LUMO and LUMO+1 orbitals, though the latter one results from the mixture of several Slater's determinants.

3. Excited States of the Second Metastable State MS_I. The existence of the second metastable state MS_I has been experimentally established by Schaiquevich et al.[5] from FT-IR spectroscopy. However, the experimental UV−vis absorption of this compound has not yet been reported.

The calculated spectrum of the MS_I species is reported in Table 6. Similarly to the CpNiNO ground state, the spectrum features two bands with weak intensity located in the region of low energies (2.47 and 2.83 eV), both of E_1 symmetry. These two peaks consist of similar electron transitions, namely, the {HOMO−2,HOMO−1} → LUMO ones and the determinants involved in the transitions have reverse contributions. Two higher energy peaks appear at 3.73 and 5.46 eV, both of A_1 symmetry and with similar intensity. The band at 3.73 eV corresponds to the HOMO−LUMO transition whereas the one at 5.46 eV is composed of a mixture of three transitions, namely, the HOMO−6 → LUMO, HOMO−3 → LUMO, and HOMO−LUMO ones.

In conclusion, the spectrum of the MS_I species is very similar to that of the ground state, though somewhat dowshifted.

IV. Discussion

To interpret the photochemical processes which occur during the forward and backward reactions, the geometries of the excited states pertaining to the reactions have been fully optimized.

A. Photochemical Processes: Forward Reactions. According to the calculated UV spectrum of the ground state CpNiNO (Table 4) one can see that the electronic excitation which is responsible for the appearance of the first metastable state MS_{II} is the HOMO−LUMO one, as it is intense and energetically low. Furthermore, as the HOMO and LUMO orbitals of the GS species are doubly degenerated, it is expected that a vibronic coupling effect (pseudo Renner−Teller) will break the symmetry of the molecule so as to lower the energy of the excited state. From the C_{5v} to the C_s symmetry, both the e_1 and e_2 orbitals split into a′ and a″ representations. As depicted in Figure 5, the

Table 7. Geometrical Parameters of Ground, Metastable, and Excited States of the CpNiNO Complex[a]

parameters	NiN	NiO	NO	XNi[b]	NiNO	NiON	XNiN[b]	XNiO[b]	Cp plane−XNi[c]
GS	162.9	344.	118.1	176.3	180.	0.	180.	180.	90.0
r-ExSt$_{GS}$	177.4	278.9	120.4	179.7	138.1	25.1	156.7	171.6	89.3
TS$_{II}$	167.6	251.7	119.4	182.	121.7	34.6	159.5	178.2	87.0
MS$_{II}$	172.1	209.	123.	177.	88.6	55.4	153.1	170.9	93.2
r-ExSt$^{1l}_{MS_{II}}$	176.3	292.8	119.8	184.4	162.6	10.3	155.5	148.4	86.9
r-ExSt$^{1r}_{MS_{II}}$	192.7	186.5	127.3	178.	67.8	76.1	155.5	165.3	88.7
r-ExSt$^{2l}_{MS_{II}}$	176.3	295.8	119.5	192.0	177.9	1.3	178.7	179.6	85.5
r-ExSt$^{2r}_{MS_{II}}$	196.6	199.7	124.7	189.2	73.0	70.0	159.9	163.4	88.4
r-ExSt$^{3l}_{MS_{II}}$	176.5	291.2	119.9	192.2	158.2	13.0	172.0	163.2	97.5
r-ExSt$^{3r}_{MS_{II}}$	290.9	188.6	121.7	194.4	25.5	138.3	180.0	163.9	101.1
r-ExSt$^{4l}_{MS_{II}}$	183.8	192.3	121.2	289.2	75.1	67.4	163.5	159.0	36.4
r-ExSt$^{4r}_{MS_{II}}$	287.2	179.0	122.6	159.9	21.6	143.8	153.1	167.6	48.0
r-ExSt$^{5l}_{MS_{II}}$	167.2	287.4	120.4	245.6	176.0	2.3	158.6	160.3	125.0
r-ExSt$^{5r}_{MS_{II}}$	187.6	177.0	122.3	240.9	19.4	147.3	152.4	165.6	122.8
TS$_{I}$	265.	172.4	119.3	182.5	30.	129.7	175.3	164.4	86.4
MS$_{I}$	287.5	169.2	118.3	176.3	0.	180.	180.	180.	90.0
r-ExSt$_{MS_I}$	277.4	187.0	120.7	189.4	32.4	127.4	163.4	143.2	102.9

[a] GS = ground state. r-ExSt = relaxed excited state. TS = transition state. MS = metastable state. [b] X = ghost atom which is the barycenter of the carbon ring. [c] Angle between the Cp plane and the XNi axis.

pseudo Renner−Teller effect is most active for the a′ → a′ electronic transition, leading to the lowest energy state. On the contrary, the a″ → a″ transition is not coupled with the NiNO bending mode. The location of the HOMO−LUMO excited state of the GS species is depicted in Figure 1 and labeled r-ExSt$_{GS}$. The NiNO angle corresponding to this structure is very close to that of the TS$_{II}$ species (121.7° and 138.1°, respectively: Table 7). The torsion which leads to MS$_{II}$ is strongly initiated in the relaxed excited state. As to the energy difference between those structures, it amounts to only 0.13 eV. Therefore, upon nonradiative relaxation, the excited state can lead to either the ground state or the metastable state MS$_{II}$. Considering the relative position of r-ExSt$_{GS}$ to that of TS$_{II}$ (by comparing the NiNO angle), it is expected that the amount of GS obtained after relaxation of the excited state is more important than that of MS$_{II}$. This may explain why the UV spectrum of the MS$_{II}$ species has not been clearly detected yet. Though some bands of MS$_{II}$ are intense, they can be hidden by those of GS as they appear in the same range of energies.

From the MS$_{II}$ state both the forward and backward reactions are possible. We shall consider the forward reaction toward the MS$_{I}$ species.

For this state, five vertical excited configurations have been calculated. They are labeled v-ExSt$^{1}_{MS_{II}}$, v-ExSt$^{2}_{MS_{II}}$, v-ExSt$^{3}_{MS_{II}}$, v-ExSt$^{4}_{MS_{II}}$, and v-ExSt$^{5}_{MS_{II}}$ in Figure 1. They correspond to the main transition involved in the absorption bands reported in Table 5, namely the HOMO → LUMO, HOMO−3 → LUMO, HOMO−2 → LUMO+1, HOMO−5 → LUMO, and HOMO−6 → LUMO+1 ones. Among all these excitations, the HOMO−LUMO one is the only one which leads to a configuration lying lower in energy than the TS$_{I}$ structure. Therefore, the HOMO−LUMO excitation cannot lead to the second metastable state. For the sake of completeness the geometric relaxation of the HOMO−LUMO excited configuration (labeled r-ExSt$^{1,r}_{MS_{II}}$ in Figure 1) has been performed. The resulting structure lies 0.96 eV lower in energy than the transition state TS$_{I}$.

As already mentioned, the next four excited states are higher in energy than TS$_{I}$. The r-ExSt$^{2,r}_{MS_{II}}$ is ca. 0.55 eV above the barrier. However, the NiON angle of r-ExSt$^{2,r}_{MS_{II}}$ is much smaller than that of TS$_{I}$ (70.3° and 129.7°, respectively).

In Figure 1 are depicted the r-ExSt$^{3,r}_{MS_{II}}$, the r-ExSt$^{4,r}_{MS_{II}}$, and the r-ExSt$^{5,r}_{MS_{II}}$ species. These three excited states are much higher in energy than the transition state, i.e. 0.91, 1.82, and 2.13 eV, respectively. Furthermore, compared with the position of TS$_{I}$ they are located beyond the barrier. Consequently, upon excitation of the MS$_{II}$ species, all of these excited states may lead to the second metastable state MS$_{I}$. However, whereas the r-ExSt$^{3,r}_{MS_{II}}$ state corresponds to a η^5(Ni−Cp) structure, both the r-ExSt$^{4,r}_{MS_{II}}$ and the r-ExSt$^{5,r}_{MS_{II}}$ are quasi dissociated as their structures are a η^1(Ni−Cp) and η^2(Ni−Cp) one, respectively (see Table 7 for the geometrical parameters).

B. Photochemical Processes: Backward Reactions. Once the second metastable MS$_{I}$ has been reached, the system can undergo the reverse GS ← MS$_{II}$ ← MS$_{I}$ reaction. From the MS$_{I}$ state the first excited state which is a good candidate for the backward reaction is the HOMO−LUMO one. Similarly to the ground state, the HOMO−LUMO excited state of MS$_{I}$ is rather low in energy, though higher than the TS$_{I}$ structure by about 0.80 eV (see Figure 1). Furthermore, the vertical transition is the first most intense transition (see Table 6). The electronic structure of MS$_{I}$ is very similar to that of GS. Upon excitation, the vibronic coupling leads to the splitting of the HOMO and LUMO orbitals and to the descent in symmetry of the excited state. As for the relaxed excited state, the energetic contribution of the pseudo Renner−Teller effect has been quantified, and it amounts to 0.42 eV. The r-ExSt$_{MS_I}$ structure is then still higher in energy than the barrier of the reverse reaction. As depicted in Figure 1, it is noteworthy that the NiON angle of TS$_{I}$ is larger than that of the r-ExSt$_{MS_I}$ species (129.7° and 127.4°: Table 7). Consequently, the r-ExSt$_{MS_I}$ structure not only is higher in energy than the barrier but also is located beyond this barrier. This involves an important difference compared with the ground state situation. From these behaviors, one may assume that the reverse MS$_{II}$ ← MS$_{I}$ reaction is more efficient that the forward GS → MS$_{I}$ reaction.

It remains to study the backward GS ← MS$_{II}$ reaction. Similarly to the forward reaction, all the relaxed structures of the excited states have been calculated. The positions of these structures are depicted in Figure 1 and are labeled with an "l" as exponent. One can see that, for all the excited states, the geometric relaxation leads to a state which is both higher in energy than the transition state TS$_{II}$ and beyond the barrier (i.e., the NiNO angle of the relaxed excited state is smaller than that of TS$_{II}$). Therefore one can assume that, whatever the energy involved in the excitation of the sample, the backward GS ← MS$_{II}$ reaction is more efficient than the forward MS$_{II}$ → MS$_{I}$

Table 8. Hirshfeld and Mulliken Charge Analysis along the Ni−N−O ↔ Ni−O−N Potential Energy Curves

	GS	TS_{II}	MS_{II}	TS_I	MS_I
			CpNiNO		
Hirshfeld					
Ni	0.26	0.33	0.32	0.30	0.27
Cp	−0.14	−0.22	−0.15	−0.23	−0.17
N	−0.05	−0.05	−0.07	−0.03	−0.06
O	−0.07	−0.06	−0.10	−0.04	−0.04
NO	−0.12	−0.11	−0.17	−0.07	−0.10
Mulliken					
Ni	0.10	0.16	0.20	0.22	0.17
Cp	0.04	−0.06	0.03	−0.09	0.02
N	0.06	0.10	0.02	0.05	−0.01
O	−0.20	−0.20	−0.26	−0.19	−0.16
NO	−0.14	−0.10	−0.24	−0.14	−0.17

Table 9. Energy Gradients along the Ni−N−O ↔ Ni−O−N Potential Energy Curve[a]

exc state no.	GS	MS_{II}	MS_I
5		0.18 (l)	
4		0.06 (r)	
3		0.15 (l)	
2		0.18 (r)	
1	0.17 (r)	0.21 (r)	0.15 (l)

[a] In the case of MS_{II}, left (l) or right (r) indicates the direction of spontaneous relaxation toward the GS or the MS_I structures.

reaction. However, the geometrical relaxation of the v-$ExSt^5_{MS_{II}}$ toward the GS leads to a quasi dissociated structure, namely, a η^2(Ni−Cp) one.

From a practical point of view, it is of major importance to understand in which direction the excited states of MS_{II} can spontaneously relax. To have a first idea of this behavior, the relaxation of the excited states has been performed retaining the geometric structure of MS_{II} with the electronic configuration of the corresponding excited state as a starting point. Hence, it has been evidenced that the two lowest excited states and the fourth one relax toward the MS_I structure whereas the v-ExS$t^3_{MS_{II}}$ and the v-$ExSt^5_{MS_{II}}$ excited states relax toward the GS species. Consequently, a crude interpretation of these results allows us to assume that the only excited state which is able to generate the MS_I species is the v-$ExSt^2_{MS_{II}}$ one. Since the r-ExS$t^4_{MS_{II}}$ and the r-$ExSt^5_{MS_{II}}$ are dissociated-like structures, the excitation window to lead to MS_I is very narrow (around 3.32 eV). However, the potential energy surface near the v-$ExSt^2_{MS_{II}}$ species exhibits one of the greatest gradients (0.18 Ry·Å^{-1}) compared to those of the other vertically excited states, as can be seen from Table 8. It is obvious that the larger the gradient (toward one side), the smaller the probability for the complex to relax toward the opposite site (uphill) thanks to a favorable vibronic coupling.

C. About a Supposed Charge Transfer. It has been stated[2] that the formation of the MS_{II} species results from a charge transfer according to the scheme $Cp^{(-)}Ni^{(0)}NO^{(+)} \rightarrow Cp^{(-)}Ni^{(2+)}NO^{(-)}$. Actually, the Mulliken and Hirschfeld charges analysis (Table 9) shows that this assumption is not strictly verified as the charge on each ligand does not change drastically through the rotation of the NO group of atoms. In particular, the charge on NO is always negative along the path whereas it changes from positive to negative according to the previous scheme. However, it can be noticed that, though the MS_{II} state results from an excited state which undergoes a Cp → NO charge transfer (i.e., the HOMO−LUMO transition of GS), Table 9 shows that the excess of charge on NO in MS_{II} seems to originate from the nickel center since the charge on Cp remains similar in GS and MS_{II} structures. In fact, the GS → MS_{II} reaction can be interpreted as follows: Upon excitation of the GS, part of the electron density is transferred from the Cp ligand to the NO one. The excited state relaxes and decays toward the TS_{II} species. At this stage, it can be seen that the decay has mainly enriched the Cp ligand in electrons whereas the electronic population of the Ni atom has decreased. Along the TS_{II} → MS_{II} path the electron density is transferred from the Cp ligand to the NO one, whereas the charge on the Ni atom remains unchanged. Consequently, one can assume that the GS → MS_{II} reaction is mainly (but rather small) a Cp → NO charge transfer.

V. Concluding Remarks

In this work the photochemistry of the CpNiNO complex has been investigated. It has been shown that the three minima, with increasing energies going from GS to MS_I, are connected by two transition states, the first one being lower in energy than the second one. As the last barrier is energetically high, this may explain why the MS_I species has not been experimentally detected for a long time.

As the GS and MS_I species have similar geometrical structures (C_{5v} symmetry with linear NiNO group of atoms) as well as electronic ones, the forward GS → MS_{II} reaction and the backward MS_I ← MS_{II} one occur with a similar excited state as intermediate, namely, the HOMO−LUMO one. Furthermore, both of these excited states are higher in energy than the barrier. However, whereas the r-$ExSt_{MS_I}$ excited state is geometrically located beyond the barrier, this is not the case for the r-$ExSt_{GS}$ excited state. Consequently, we assume that the GS → MS_{II} reaction is less efficient than the MS_I ← MS_{II} one.

Finally, thermal excitation of MS_{II} allows easy crossing of the energy barrier toward the GS (0.4 eV), whereas the energy barrier toward MS_I is significantly higher (1.64 eV) so that the probability to obtain MS_I is smaller than 2% with respect to the transformation toward the GS. Photochemical excitations of MS_{II} lead to (a) v-$ExSt^1_{MS_{II}}$, with a small absorption coefficient, which rearranges into a structure between TS_I and MS_{II}, leading back to MS_{II}; (b) v-$ExSt^3_{MS_{II}}$, with a small absorption coefficient, which rearranges into a structure between GS and TS_{II}, leading to GS; (c) v-$ExSt^4_{MS_{II}}$ and v-$ExSt^5_{MS_{II}}$, with a high absorption coefficient, which rearranges either into a quasi dissociated structure on the right-hand side of the PEC or into a dissociative state at the vertical of GS, respectively; and (d) v-$ExSt^2_{MS_{II}}$, with a unique favorable (though small) absorption coefficient, which requires near-UV light (373 nm). This is the unique excited state which is able to rearrange into MS_I.

Therefore, the photochemical obtention of MS_I is rather difficult, and that is the reason why it has not been experimentally identified until recently. This contrasts with the sodium nitroprusside system which is able to give the MS_I state through HOMO−LUMO excitation of the MS_{II}.[23]

Acknowledgment. The authors would like to thank Prof. Andreas Hauser (Geneva) and Prof. Claude Daul (Fribourg) for fruitful discussions. This work has been supported by the Swiss National Science Foundation (Grant 2-55459.98).

IC010489C